

# Controlled Aliasing in Volumetric Parallel Imaging (2D CAIPIRINHA)

Felix A. Breuer,\* Martin Blaimer, Matthias F. Mueller, Nicole Seiberlich, Robin M. Heidemann, Mark A. Griswold, and Peter M. Jakob

**The CAIPIRINHA (Controlled Aliasing In Parallel Imaging Results IN Higher Acceleration) concept in parallel imaging has recently been introduced, which modifies the appearance of aliasing artifacts during data acquisition in order to improve the subsequent parallel imaging reconstruction procedure. This concept has been successfully applied to simultaneous multi-slice imaging (MS CAIPIRINHA). In this work, we demonstrate that the concept of CAIPIRINHA can also be transferred to 3D imaging, where data reduction can be performed in two spatial dimensions simultaneously. In MS CAIPIRINHA, aliasing is controlled by providing individual slices with different phase cycles by means of alternating multi-band radio frequency (RF) pulses. In contrast to MS CAIPIRINHA, 2D CAIPIRINHA does not require special RF pulses. Instead, aliasing in 2D parallel imaging can be controlled by modifying the phase encoding sampling strategy. This is done by shifting sampling positions from their normal positions in the undersampled 2D phase encoding scheme. Using this modified sampling strategy, coil sensitivity variations can be exploited more efficiently in multiple dimensions, resulting in a more robust parallel imaging reconstruction. Magn Reson Med 55:549–556, 2006. © 2006 Wiley-Liss, Inc.**

**Key words:** volumetric parallel imaging; controlled aliasing; CAIPIRINHA; SENSE; GRAPPA

Image acquisition time is one of the most important considerations for clinical magnetic resonance imaging (MRI). In recent years, the concept of partially parallel acquisition (PPA) enabled great progress in increasing imaging speed. PPA operates by reducing the number of required phase encoding steps. In the Cartesian case, this is usually done by uniformly undersampling  $k$ -space, while maintaining the maximum  $k$ -values in order to retain full resolution. Several PPA reconstruction strategies have been developed (1–7) that use the spatial sensitivity information provided by multiple receiver coils to compensate for the lack of spatial encoding normally obtained via phase encoding gradients. Unfortunately, the PPA strategy is intrinsically associated with a signal-to-noise (SNR) loss and, therefore, limited to applications with high SNR, such as volumetric imaging methods.

With the newest generation of MR-scanners providing up to 32 independent receiver channels, further scan time reductions are potentially achievable. However, in conventional 2D imaging, parallel imaging is restricted to relatively small scan time reductions due to intrinsic limitations in the coil sensitivity variations along one phase encoding direction (1D parallel imaging). In 3D and simultaneous multi-slice imaging, parallel encoding can be carried out in two encoding directions (2D parallel imaging), thereby exploiting the sensitivity variations in both directions, as in, for example, 2D SENSE (8) and MS SENSE (9). This concept has been shown to significantly improve the reconstruction conditions, allowing higher image accelerations. However, both techniques require sufficient sensitivity variations in two encoding directions for successful image reconstruction and, therefore, strongly depend on the underlying coil geometry. Recently, we have shown that these requirements in simultaneous multi-slice imaging can be partially overcome by shifting the individual slices with respect to each other in a controlled manner (MS CAIPIRINHA (10)). This is performed by excitation with alternating multi-band radio frequency (RF) pulses, similar to Hadamard pulses. In this work, a encoding strategy for 2D parallel imaging is presented where the concept of CAIPIRINHA is applied to 3D volume imaging (11).

Besides the standard 2D SENSE (8) sampling patterns, where rectangular undersampling is performed using simple integer reductions in each direction, many other patterns are conceivable where the sampling positions are shifted from their original positions in the 2D phase encoding scheme, as also proposed recently by others (12–14). These shifts are attained by applying additional gradient offsets to the phase encoding gradient tables. In this study, 2D CAIPIRINHA is presented, which modifies the appearance of aliasing in 2D parallel imaging by using these modified 2D phase encoding patterns. We show that by shifting sampling positions in a well-directed manner, aliasing can be shifted in such a way that sensitivity variations provided by the underlying receiver array can be exploited more efficiently. These modified aliasing conditions then result in a further improvement in parallel imaging reconstruction conditions and, therefore, in better image quality. Although image reconstructions are performed using the SENSE algorithm, other standard PPA reconstruction algorithms, such as GRAPPA, could be used as well.

## THEORY

### A Simple Example

In order to clarify 2D parallel imaging and in particular to explain how aliasing can be controlled in 2D parallel im-

University of Würzburg, Department of Experimental Physics 5, Würzburg, Germany.

Grant Sponsor: Deutsche Forschungsgemeinschaft; Grant Number: DFG, JA 827/4. Grant Sponsor: Siemens Medical Solutions.

\*Correspondence to: Felix Breuer, University of Würzburg, Department of Physics, EP 5, Am Hubland, 97074 Würzburg, Germany. E-mail: fxbreuer@physik.uni-wuerzburg.de

Received 20 April 2005; revised 19 September 2005; accepted 25 October 2005.

DOI 10.1002/mrm.20787

Published online 11 January 2006 in Wiley InterScience (www.interscience.wiley.com).

© 2006 Wiley-Liss, Inc.

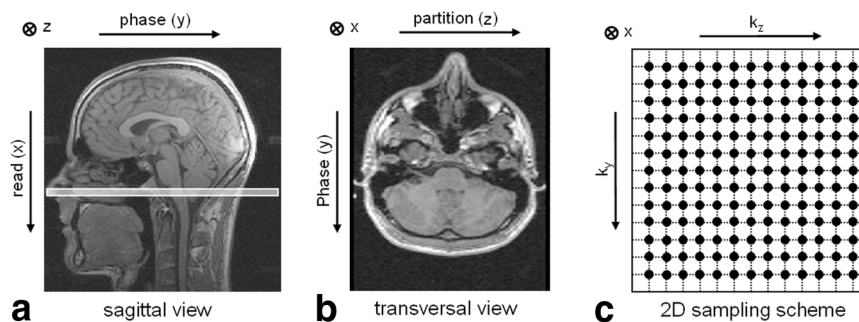


FIG. 1. (a) One partition of a fully encoded 3D imaging experiment is displayed in the sagittal view with normal phase encoding (phase) in the AP direction and frequency encoding (read) in the HF direction. The second phase encoding direction (partition) is in-plane in the LR direction. (b) In the transversal view, both phase encoding directions (phase and partition) can be displayed simultaneously in one plane. (c) Additionally, the corresponding fully encoded 2D sampling pattern is displayed. Each dot represents a phase-encoded read-out line in the HF direction.

aging (2D CAIPIRINHA), we begin with a brief review of conventional unaccelerated 3D volume imaging.

In Fig. 1a, one sagittal partition taken from a fully encoded 3D volume experiment is shown. The normal phase encoding direction is chosen to be in the anterior-posterior (AP) direction ( $y$ ), the second phase encoding direction (partition encoding direction) in the left-right (LR) direction ( $z$ ), and the frequency encoding direction in the head-foot (HF) direction ( $x$ ). In order to better visualize how undersampling in two dimensions affects the appearance of aliasing, it is useful to switch from the sagittal to the transversal view (Fig. 1b). Now both phase encoding directions are displayed simultaneously in one plane. In Fig. 1c, a schematic depiction of the corresponding fully encoded 2D sampling pattern is given, where each dot represents a phase-encoded read-out line.

For illustration purposes, it is useful to start with a simple example of a two-times undersampled parallel acquisition. In conventional 2D parallel imaging, given a reduction factor  $R = 2$ , two different sampling patterns are possible. The reduction can either be performed only in the normal phase encoding direction ( $R_y = 2, R_z = 1$ ) or only in the partition encoding direction ( $R_y = 1, R_z = 2$ ). The resulting aliasing artifacts appear only in the undersampled dimension. In Fig. 2, both scenarios are shown in more detail. Besides schematics of both undersampled 2D acquisition schemes (Fig. 2, left), the corresponding 2D aliasing patterns are illustrated in the  $yz$ -plane showing a masked section of the head. Additionally, a single partition of each aliased data set, indicated by the vertical line, is shown in the sagittal view (Fig. 2, right). As can be seen, after a simple reduction by a factor of  $R_y = 2$  in the normal

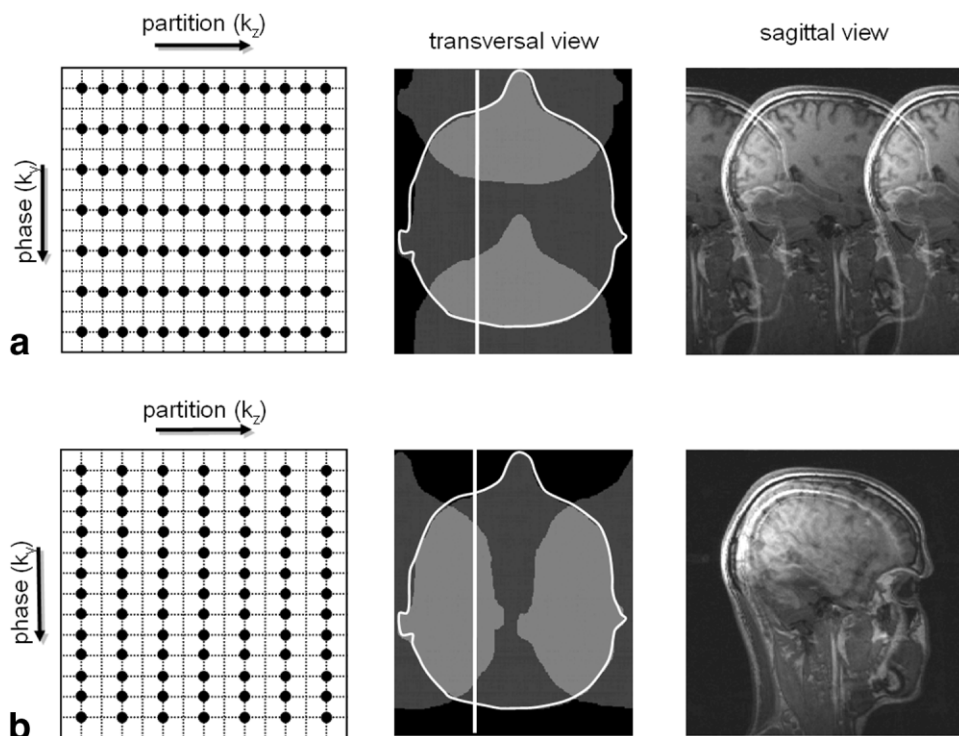
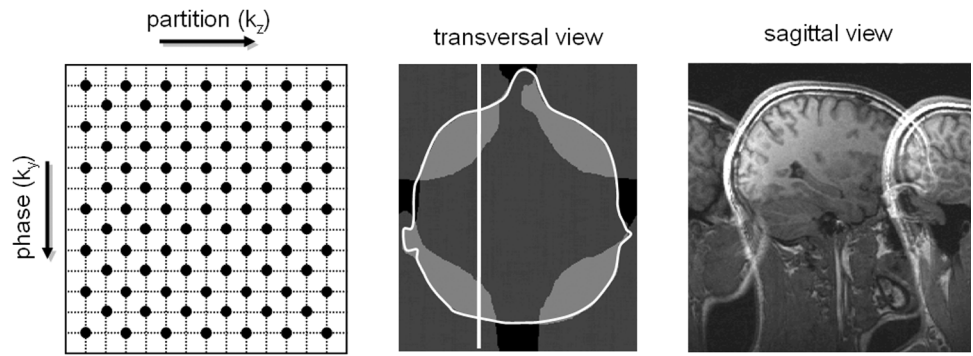


FIG. 2. Undersampling by a factor  $R = 2$  in 3D imaging can be performed either (a) in the normal phase encoding direction or (b) in the partition encoding direction. On the left-hand side, the corresponding twofold undersampled phase encoding schemes are shown. The resulting aliasing conditions are demonstrated for each scenario by means of a masked section of the head in the transversal plane (middle). In addition, one arbitrary section of the reduced data set, indicated by the vertical bar, is displayed in the sagittal view (right).

FIG. 3. 2D CAIPIRINHA-type experiment ( $R = 2$ ). Starting at scenario 1 given in Fig. 2a, every second phase encoding table in the  $k_y$  direction is shifted by  $\Delta k_z$  in the  $k_z$  direction. This modification of the sampling pattern directly results in modified aliasing conditions, which are displayed in the transversal and the sagittal views.



phase encoding direction (Fig. 2a), each partition is aliased two times in the y-direction. On the other hand, after a simple reduction by  $R_z = 2$  in the partition encoding direction (Fig. 2b), two partitions are superimposed directly on top of each other. This scenario corresponds to the two times accelerated ( $R = 2$ ) simultaneous two-slice SENSE experiment, where both slices are also aliased directly on top of each other.

However, another  $R = 2$  undersampled sampling pattern is possible. For example, starting from the  $R_z = 2$  case given in Fig. 2b, a pattern similar to the scheme given in Fig. 3 (left) can be generated by applying gradient offsets to every second gradient table in the phase encoding direction in order to shift the sampling positions exactly by  $\Delta k_z$ . The corresponding 2D aliasing (Fig. 3, middle) is different from the two former scenarios. In the sagittal view, the difference is obvious; the same partitions are superimposed directly on top of each other, but now they are shifted in the y-direction with respect to each other. This scenario is identical to the two-times accelerated ( $R = 2$ ) simultaneous two-slice CAIPIRINHA experiment, where

both slices are superimposed, but shifted with respect to each other in the phase encoding direction.

### Optimized CAIPIRINHA Sampling Patterns in Volumetric Parallel Imaging

With higher reduction factors, the number of possible 2D sampling patterns (SP) increases. In the following section, we restrict ourselves to sampling positions on a Cartesian grid. For simplicity, in Fig. 4 only an  $R \times R$  section of the entire sampling scheme is shown, where  $R$  represents the total reduction factor. In order to achieve a periodic R-fold undersampled 2D acquisition, R sampling points can be arbitrarily distributed in the elementary  $R \times R$  cell, yielding  $\frac{R^2!}{(R^2 - R)!}$  possibilities. However, in order to minimize the number of image pixels aliased on top of each other due to undersampling, we confine ourselves to sampling positions on so-called sheared grids that form periodic lattices (13,15). Thus, as a result of the corresponding two dimensional point spread functions (PSF), a maximum of

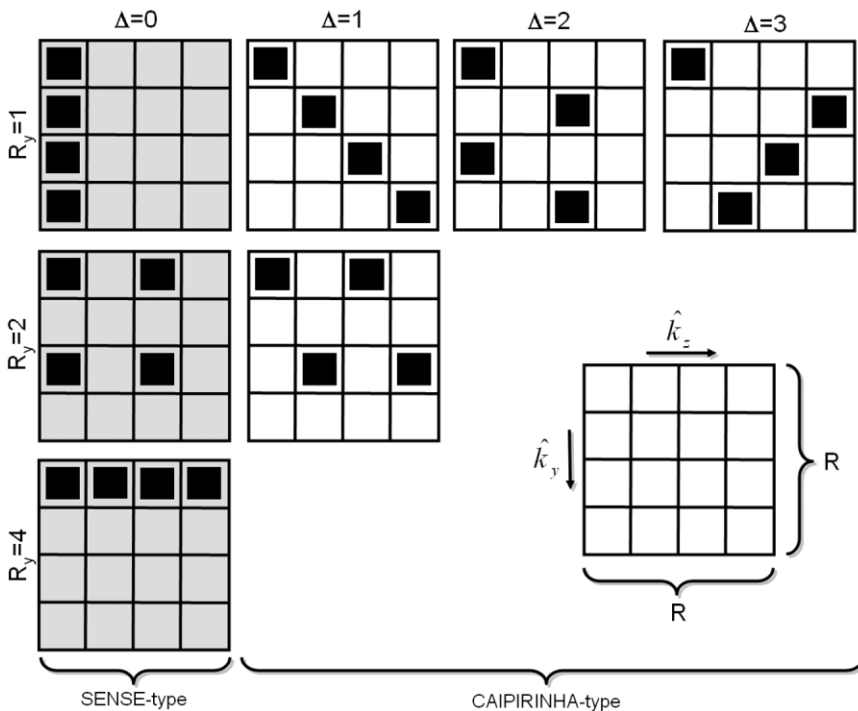


FIG. 4. Complete set of acceptable sampling patterns given a reduction factor of  $R = 4$ . The sampling patterns can be represented by an  $R \times R$  elementary cell with R sampling positions to fill. For each undersampling rate in the  $k_y$  direction ( $R_y$ ) multiple patterns can be created by shifting sampling positions at row  $k_y$  in the  $k_z$  direction by a different amount  $\Delta$ , whereas  $\Delta$  runs from 0 to  $R_z - 1$ , where  $R_z = R/R_y$ . Sampling patterns with no shift ( $\Delta = 0$ ) are 2D SENSE-type acquisitions, while all the other patterns are represented by 2D CAIPIRINHA-type experiments.

Table 1  
Possible Undersampling Rates ( $R_y$ ) for Several Total Reduction Factors  $R$

R	2	3	4	5	6	7	8	9	10	11	12	13	14	15	16
$R_y$	1	1	1	1	1	1	1	1	1	1	1	1	1	1	1
	2	3	2	5	2	7	2	3	2	11	2	13	2	3	2
			4		3		4	9	5		3		7	5	4
					6		8		10		4		14	15	8
											6				16
											12				
#SP	3	4	7	6	12	8	15	13	18	12	28	14	24	24	31

For each  $R_y$ ,  $R_z = R/R_y$  different sampling patterns (SP) are possible, resulting in the total number of acceptable sampling schemes (#SP) given in the last row.

$R$  pixels are aliased together in one single pixel. Additionally, without loss of generality, only patterns starting at sampling position (1,1) in the binary sampling cell are considered. This arrangement leads to a reduced number of acceptable undersampled 2D sampling patterns.

In order to find the complete set of patterns given a specific reduction factor  $R$ , one arbitrary dimension (e.g.,  $y$ ) can be selected, in which certain degrees of undersampling (e.g.,  $R_y$ ) can be defined. For example, at a given total reduction factor of  $R = 4$ , the undersampling rate  $R_y$  can take values of  $R_y = 1, 2, 4$ . For each  $R_y$  a certain number of sampling patterns can be created by shifting successive sampling positions in  $k_y$  with respect to each other by a factor  $\Delta$  in the  $k_z$  direction (see Fig. 4). If a sampling position exceeds  $R$  due to the shift, it is wrapped around in the elementary cell. In the end, this strategy leads us to all acceptable 2D sampling patterns. The patterns at a certain undersampling rate  $R_y$  are limited to  $R/R_y$ , with shifts  $\Delta$  running from 0 to  $R/R_y - 1$ . Shifts  $\Delta$  greater than  $R/R_y - 1$  will result in repetitive patterns. In Table 1, all possibilities for  $R_y$  are listed for several total reduction factors ( $R = 1$  to 16). Furthermore, the corresponding total number of possible sampling patterns given a specific total reduction factor  $R$  is shown (last row).

The procedure, for creating a complete set of possible sampling patterns is illustrated in Fig. 4 for a reduction factor of  $R = 4$ . The first row represents all cases in which  $R_y = 1$ , with shifts  $\Delta = 0, 1, 2, 3$ . In the second row, alternative patterns using  $R_y = 2$  with shifts  $\Delta = 0, 1$  are listed. Finally, the remaining  $R_y = 4$  case with  $\Delta = 0$  is displayed.

In general, in this Figure, 2D SENSE-type ( $R_{SENSE} = R_y \times R_z$ ) patterns are listed in the first column without a shift ( $\Delta = 0$ ), while all other sampling schemes are characterized by 2D CAIPIRINHA type acquisitions including various shifts. For differentiation purposes, 2D CAIPIRINHA-type reduction factors are specified as

$$R_{CAIPI} = R_y \times R_z^{(\Delta)} \quad [1]$$

with  $\Delta$  representing the applied shift in the  $k_z$  direction from one sampling row  $k_y$  to the next, and  $R_z = R/R_y$ .

#### Reconstruction Procedure

The first step in reconstruction is the creation of a binary  $R \times R$  matrix, where sampling positions are set to 1 and skipped positions are set to 0. After 2D Fourier transformation of such an  $R$ -fold undersampled elementary  $R \times R$  cell, the corresponding binary 2D point-spread function (see Fig. 5) is obtained, which leads us directly to the originating spatial locations of the  $R$  signals aliased together in one pixel. By means of the  $R$  matrix indices ( $\hat{y}_l, \hat{z}_l$ ) with value 1 in the binary aliasing cell, the  $R$  spatial locations ( $y_l, z_l$ ) in the 2D FOV and, therefore, the involved sensitivity values can directly be determined:

$$(y_l, z_l) = \left( y + (\hat{y}_l - 1) \cdot \frac{FOV_y}{R}, z + (\hat{z}_l - 1) \cdot \frac{FOV_z}{R} \right), \quad l = 1, \dots, R \quad [2]$$

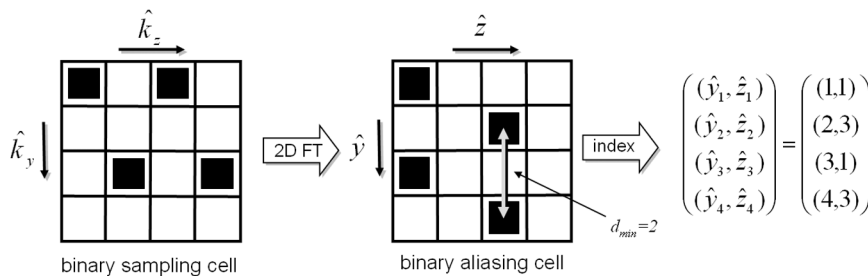


FIG. 5. Schematic description of a 2D CAIPIRINHA reconstruction procedure. A 2D Fourier transform of the binary sampling cell directly yields the corresponding 2D point spread function. The minimum distance of points in the aliasing cell  $d_{min}$  is a measure of the quality of the point spread function (PSF). The  $R$  indices ( $y_l, z_l$ ) with value 1 in the resulting elementary aliasing cell allow one to determine the  $R$  pixels at the spatial locations ( $y_l, z_l$ ) that are aliased in one pixel (see Eq. [2]) and the involved coil sensitivity values that are needed for the following SENSE reconstruction procedure.

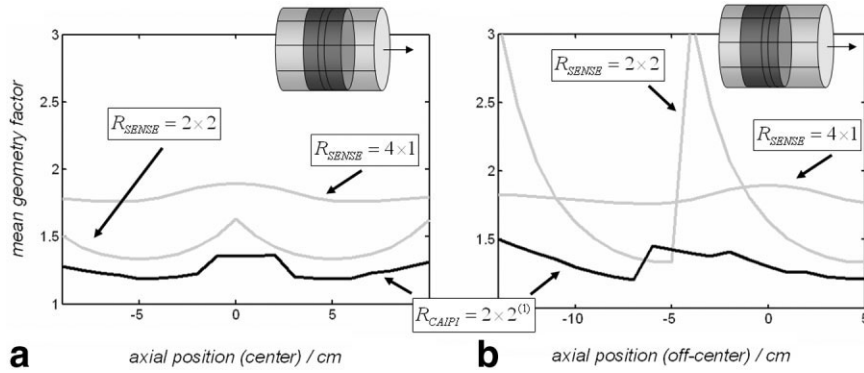


FIG. 6. Results of several fourfold accelerated 2D parallel imaging experiments, exploiting the sensitivity distribution of a simulated cylindrical 16-channel two ring head array. The mean geometry factor as a function of the axial partition position after 2D SENSE ( $R_{SENSE} = 4 \times 1$  and  $R_{SENSE} = 2 \times 2$ ) and 2D CAIPIRINHA ( $R_{CAIPIRI} = 2 \times 2^{(l)}$ ) is plotted, given a 20 cm slab (a) carefully positioned in the center of the coil and (b) positioned 5 cm off-center. While the  $R_{SENSE} = 4 \times 1$  experiment has a performance that is much more independent from the slab position, the  $R_{SENSE} = 2 \times 2$  experiment performs significantly better when the slab is in the center position, as sensitivity variations are exploited in both directions simultaneously. In the off-center position, however, this acquisition strategy provides an inhomogeneous performance, with partitions showing extremely high geometry factors. In contrast, the 2D CAIPIRINHA-type experiment  $R_{CAIPIRI} = 2 \times 2^{(l)}$  provides the best reconstruction performance, with a homogeneous characteristic for both scenarios.

If the spatial locations  $y_l$  or  $z_l$  exceed  $FOV_y$  or  $FOV_z$ , they are simply wrapped around, which can be performed by applying the “modulo” function in both directions.

Using this strategy, an adapted sensitivity map is created, which can be directly provided to the normal SENSE algorithm. Finally, the output of the SENSE algorithm must be reordered according to the originating spatial locations.

## METHODS

In vivo experiments were performed on a healthy volunteer using a 1.5T clinical whole body scanner (Avanto, Siemens Medical Solutions, Erlangen, Germany) equipped with a 12 channel head array. 2D SENSE and 2D CAIPIRINHA type acquisitions were performed according to the 2D sampling patterns proposed in the Theory section (see Fig. 4). Starting with a fully encoded 3D FLASH experiment, unwanted phase encoding steps were simply removed from their sampling positions. Sensitivity information was derived from a fully encoded low-resolution data set. The two phase encoding directions were chosen to be in the AP and the LR direction. Frequency encoding was performed in the HF direction to avoid aliasing from the object outside the FOV. The sequence parameters were as follows:  $TE = 4.56ms$ ,  $TR = 12ms$ ,  $\alpha = 15^\circ$ ,  $matrix = 184 \times 192 \times 112$ ,  $FOV = 25 \times 26 \times 20$  cm. Parallel image reconstructions were performed in Matlab (The MathWorks, Natick, MA, USA) using SENSE algorithms. The modified aliasing conditions are taken into account as described in the Theory section. Geometry factor maps were also calculated as described in the original SENSE paper (3), taking noise correlations into account.

In order to further investigate the properties of 2D CAIPIRINHA, computer simulations were performed. A standard 16-channel receiver head coil array, providing not only sensitivity variations in the radial direction but also in the axial direction, was simulated (see Fig. 6). The array was made up of two cylindrical 8 coil-rings posi-

tioned in the axial direction with 2 cm overlap. The total coil dimensions were 28 cm length and 28 cm diameter. The coil sensitivity characteristics were calculated in Matlab (The MathWorks, Natick, MA, USA) using analytical Biot Savart integrations.

## RESULTS

In order to demonstrate the benefit of this approach, all 15 feasible 2D acquisition patterns (2D rectangular and 2D CAIPIRINHA-type) given a reduction factor of  $R = 8$  (see Table 1) were generated. Afterward, image reconstructions were performed using SENSE algorithms as described earlier. Additionally, g-factor maps were calculated in order to compare the reconstruction performance. In Fig. 7, parallel image reconstruction of a single transversal plane is shown after standard rectangular 2D SENSE-type accelerated in vivo head experiments (a)  $R = 2 \times 4$  and (b)  $R = 4 \times 2$ . Additionally, the 2D CAIPIRINHA SENSE-type experiment with lowest mean g-factor and lowest standard deviation (c)  $R = 1 \times 8^{(3)}$  is displayed. As can be seen, the image quality of the 2D CAIPIRINHA SENSE-type experiment is clearly superior to both rectangular 2D SENSE-type experiments due to a significantly lower geometry-related noise enhancement. This fact is even more obvious when comparing the histogram plots of the corresponding geometry factor maps. Besides a significant improvement in the mean g-factor, the histogram plots indicate a much more homogeneous reconstruction performance, which is indicated by the narrow distribution of the histogram.

In Table 2 the mean g-factor with corresponding SD and the maximum g-factor value is listed for all 15 possible sampling patterns at a reduction factor of  $R = 8$ . Additionally, the relative minimum distance  $d_{min}$  is given, which is a measure of the quality of the corresponding point spread function (PSF).  $d_{min}$  is determined by calculating the minimum distance of aliased points in the  $R \times R$  binary aliasing cell (see Fig. 5).

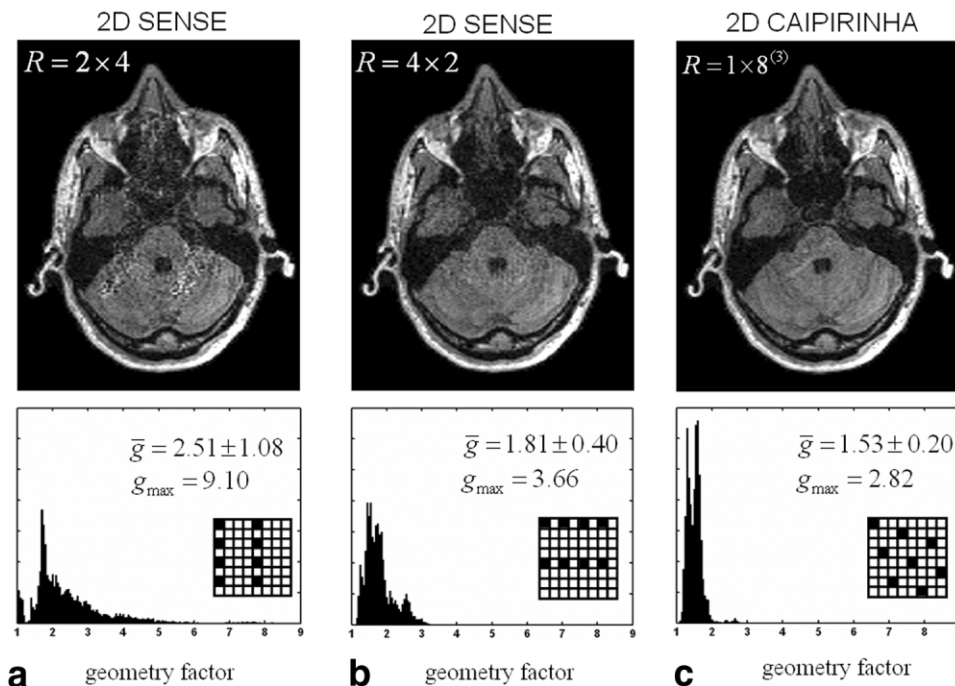


FIG. 7. In vivo results after accelerated ( $R = 8$ ) (a) 2D SENSE ( $R_{SENSE} = 2 \times 4$ ), (b) 2D SENSE ( $R_{SENSE} = 4 \times 2$ ) and (c) 2D CAIPIRINHA ( $R_{CAIP} = 1 \times 8^{(3)}$ ) experiments of the human head. As an example, image reconstructions of one transversal plane in the read-direction are shown for each experiment. Histogram plots of the corresponding g-factor maps are included to show reconstruction performance. Additionally, the mean g-factor values and their standard deviations are given for each 2D sampling scheme.

Simulation results are presented in Fig. 6 for various four-fold accelerated 2D parallel imaging experiments. The simulations were based on the sensitivity characteristics calculated from a cylindrical 16-channel head array, which has already been described in the Methods section. For all simulated scenarios, the partition encoding was chosen to be in the axial direction and an excitation slab 20 cm thick was assumed. The resulting mean and maximum geometry factors were calculated for every partition and plotted as a function of the axial partition position after 2D SENSE ( $R_{SENSE} = 2 \times 2$  and  $R_{SENSE} = 4 \times 1$ ) and 2D CAIPIRINHA SENSE ( $R_{CAIP} = 2 \times 2^{(1)}$ ) experiments. In one case (a), the excitation slab was carefully positioned in

the center of the coil; whereas in the other case (b), the slab was moved 5 cm off-center. The  $R_{SENSE} = 4 \times 1$  experiment has a performance that is much more independent from the slab position, as sensitivity variations in the axial direction are not exploited. In contrast, the 2D SENSE ( $R_{SENSE} = 2 \times 2$ ) experiment performs significantly better when the slab is positioned in the center of the coil. In this case, sensitivity variations in the partition direction, which are provided by the two ring coil geometry, can be used. In the off-center position, however, this acquisition strategy results in an inhomogeneous performance, with some partitions showing extremely high geometry factors. However, the 2D CAIPIRINHA-type experiment  $R_{CAIP} = 2 \times 2^{(1)}$  provides the best reconstruction performance and exhibits a very homogeneous g-factor behavior for both scenarios.

Table 2  
Mean Geometry Factors  $\bar{g}$  and Corresponding Standard Deviations for All 15 Sampling Schemes at a Total Reduction Factor of  $R = 8$

$R$	$\bar{g}$	$d_{min}$
$1 \times 8^{(0)}$	$25.68 \pm 19.21$	1
$1 \times 8^{(1)}$	$6.36 \pm 3.80$	1.41
$1 \times 8^{(2)}$	$1.66 \pm 0.30$	2.24
$1 \times 8^{(3)}$	$1.53 \pm 0.21$	2.83
$1 \times 8^{(4)}$	$2.51 \pm 1.17$	2
$1 \times 8^{(5)}$	$1.54 \pm 0.21$	2.83
$1 \times 8^{(6)}$	$1.65 \pm 0.27$	2.24
$1 \times 8^{(7)}$	$6.02 \pm 3.58$	1.41
$2 \times 4^{(0)}$	$2.51 \pm 1.16$	2
$2 \times 4^{(1)}$	$1.87 \pm 0.51$	2.24
$2 \times 4^{(2)}$	$1.55 \pm 0.21$	2.83
$2 \times 4^{(3)}$	$1.86 \pm 0.46$	2.24
$4 \times 2^{(0)}$	$1.81 \pm 0.41$	2
$4 \times 2^{(1)}$	$1.80 \pm 0.40$	2
$8 \times 1^{(0)}$	$14.82 \pm 10.57$	1

The minimum distances  $d_{min}$  of aliased points in the elementary aliasing cell are given.

## DISCUSSION

2D CAIPIRINHA has been presented as a means of exploiting sensitivity variations more efficiently in 2D parallel imaging. The properties of this technique were studied using computer simulations as well as in vivo studies. 2D CAIPIRINHA-type accelerated in vivo experiments were successfully performed up to reduction rates of  $R = 8$ , which still provided an acceptable SNR and image quality. The simulation results indicate that 2D CAIPIRINHA-type acquisitions have the potential to provide a more robust and homogenous reconstruction than conventional accelerated rectangular 2D SENSE and 1D SENSE-type acquisitions, even in cases where the setup is not optimized with regard to the sensitivity variations provided by the actual coil configuration.

However, at a specific reduction factor  $R$ , only one of the described 2D sampling patterns will be best suited for a given coil array, slab orientation, and object shape. At a

given total reduction factor  $R$ , multiple patterns have optimal PSFs with maximum distance of aliased points. In the case of a total reduction factor of  $R = 8$ , 3 of the 15 possible patterns have optimal PSFs. Because sensitivity variations tend to increase with increasing distance, patterns with optimal PSF are generally favorable and, therefore, one of these patterns is most likely to be best suited. However, it is clear that even the best PSF is inefficient when aliased signals with insufficient sensitivity variations are present. Since the optimal patterns are basically rotations of each other, one will quite surely exploit sensitivity variations most efficiently. Additionally, as can be seen in Fig. 3, the area with signal overlap can potentially be reduced using these optimal patterns by exploiting object-free regions inside the FOV more efficiently. Therefore, the exact sampling pattern used should be optimized beforehand, taking into account the coil array, the expected object, and FOV size. A potential strategy for finding the best sampling pattern could be to run a low resolution geometry factor analysis on the few patterns with optimal PSF, which gives the pattern with lowest mean  $g$ -factor and SD (16). Another possible approach is Principal Component Analysis (PCA) of the sensitivity information (17), which allows one to estimate the maximum possible total reduction factor  $R$  for a given coil configuration. Additionally, PCA applied to multiple directions separately, by using, for example, simple projections, allows one to determine the spatial direction with the most variations in the array.

Generally, the 2D CAIPIRINHA approach provides a broad range of applications. Especially those applications using relatively thin excitation slabs will directly benefit from this approach, such as Time-Of-Flight (TOF) angiography. Standard rectangular reduction in the partition encoding direction only helps for large excitation slabs with sufficient sensitivity variations.

2D CAIPIRINHA is easy to implement, as no special demands are made on the hardware or software. Additionally, no special RF pulses are needed to control aliasing artifacts as are required for MS CAIPIRINHA. This eliminates the main limitation of CAIPIRINHA in simultaneous multi-slice imaging, namely, the increased specific absorption rate (SAR) when exciting multiple slices simultaneously. Generally, 2D CAIPIRINHA is applicable to all common imaging techniques (FLASH, RARE, TrueFISP, EPI, etc.), and image reconstructions can be carried out using standard PPA reconstruction algorithms, such as SENSE (3) or GRAPPA (7).

Generally, the concept of CAIPIRINHA is not restricted to two dimensions. Work is currently being performed to extend this strategy to the remaining third spatial dimension. Conceivable, for example, is 3D chemical shift imaging (CSI), where a third phase encoding direction is required. With an additional phase encoding direction, the number of possible 3D sampling patterns given a specific reduction factor increases drastically. However, as in the 2D case, only one 3D sampling pattern will exploit the sensitivity variations in three dimensions most efficiently. Further strategies need to be developed that can automatically find this optimal sampling pattern.

Even in conventional volumetric parallel imaging, an additional modification of the sampling pattern in the third spatial dimension is possible. This can be realized by, for example, applying gradient blips in one phase encoding direction during the read-out process. Potential sensitivity variations in the read direction can then additionally be exploited, resulting in further improved image quality.

## CONCLUSION

In conventional PPA accelerated 3D imaging, data reduction is performed in two spatial dimensions simultaneously by integer-valued undersampling in each phase encoding direction. Though sensitivity variations can be exploited in two spatial dimensions, this sampling strategy provides suboptimal encoding performance.

In this work we presented a 2D parallel imaging strategy that takes advantage of the recently introduced concept of CAIPIRINHA (Controlled Aliasing In Parallel Imaging Results IN Higher Acceleration). Aliasing artifacts in 2D parallel imaging are modified in a controlled manner during the data acquisition by shifting sampling positions in the two dimensional phase encoding scheme with respect to each other (2D CAIPIRINHA). In this way, at certain image acceleration values, an optimal sampling pattern can be found that minimizes signal overlap and at the same time allows one to efficiently exploit the sensitivity variations provided by the coil array. This strategy provides optimal reconstruction performance given a certain coil configuration and object shape, and therefore directly results in optimal image reconstruction quality.

## REFERENCES

1. Sodickson DK, Manning WJ. Simultaneous acquisition of spatial harmonics (SMASH): fast imaging with radiofrequency coil arrays. *Magn Reson Med* 1997;38:591–603.
2. Jakob PM, Griswold MA, Edelman RR, Sodickson DK. AUTO-SMASH: a self-calibrating technique for SMASH imaging. *MAGMA* 1998;7:42–54.
3. Pruessmann KP, Weiger M, Scheidegger B, Boesiger P. SENSE: sensitivity encoding for fast MRI. *Magn Reson Med* 1999;42:952–962.
4. Heidemann RM, Griswold MA, Haase A, Jakob PM. VD-AUTO-SMASH Imaging. *Magn Reson Med* 2001;45:1066–1074.
5. Griswold MA, Jakob PM, Nittka M, Goldfarb JW, Haase A. Partially parallel imaging with localized sensitivities (PILS). *Magn Reson Med* 2000;44:602–609.
6. Kyriakos WE, Panych LP, Kacher DF, Westin CF, Bao SM, Mulkern RV, Jolesz FA. Sensitivity profiles from an array of coils for encoding and reconstruction in parallel (SPACE RIP). *Magn Reson Med* 2000;44:301–308.
7. Griswold MA, Jakob PM, Heidemann RM, Nittka M, Jellus V, Wang J, Kiefer B, Haase A. Generalized Autocalibrating Partially Parallel Acquisitions (GRAPPA). *Magn Reson Med* 2002;47:1202–1210.
8. Weiger M, Pruessmann KP, Boesiger P. 2D SENSE for faster 3D MRI. *MAGMA* 2002;14:10–9.
9. Larkman DJ, Hajnal JV, Herlihy AH, Coutts GA, Young IR, Ehnholm G. Use of multicoil arrays for separation of signal from multiple slices simultaneously excited. *J Magn Reson Imaging* 2001;13:313–317.
10. Breuer FA, Blaimer M, Heidemann RM, Mueller MF, Griswold MA, Jakob PM. Controlled Aliasing in Parallel Imaging Results in Higher Acceleration (CAIPIRINHA) for Multislice Imaging. *Magn Reson Med* 2005;53:684–691.

11. Breuer F, Blaimer M, Mueller M, Heidemann R, Griswold M, Jakob P. Controlled Aliasing in Parallel Imaging Results In Higher Acceleration (CAIPIRINHA). In: Proceedings of the 20th Annual Meeting of ESMRMB, Rotterdam, Netherlands, 2003. p 40.
12. Breuer F, Blaimer M, Mueller M, Heidemann R, Griswold M, Jakob P. Controlled aliasing in 3D parallel imaging (2D CAIPIRINHA). In: Proceedings of the 12th Annual Meeting of ISMRM, Kyoto, Japan, 2004. p 326.
13. Tsao J, Kozerke S, Hansen MS, Boesiger P, Pruessmann KP. Optimized canonical sampling patterns in k-t space with two and three spatial dimensions for k-t BLAST and k-t SENSE. In: Proceedings of the 12th Annual Meeting of ISMRM, Kyoto, Japan, 2004. p 261.
14. Jurrissen M, Fuderer M, van den Brink J. Diamond-SENSE: undersampling on a crystallographic grid. In: Proceedings of the 12th Annual Meeting of ISMRM, Kyoto, Japan, 2004. p 2643.
15. Willis NP, Bresler Y. Optimal scan design for time varying tomographic imaging (II): Efficient design and experimental validation. *IEEE Trans Image Processing* 1995;4:654–666.
16. Breuer FA, Blaimer M, Heidemann RM, Mueller MF, Griswold MA, Jakob PM. Finding the optimal sampling pattern in 2D parallel imaging for a given receiver coil configuration. In: Proceedings of the 13th Annual Meeting of ISMRM, Miami Beach, FL, USA, 2005. p 2665.
17. Breuer FA, Blaimer M, Heidemann RM, Mueller MF, Griswold MA, Jakob PM. The use of Principal Component Analysis (PCA) for estimation of the maximum reduction factor in 2D parallel imaging. In: Proceedings of the 13th Annual Meeting of ISMRM, Miami Beach, FL, USA, 2005. p 2668.